This manuscript "Fast anisotropic Mg and H diffusion in wet forsterite" is a preprint manuscript uploaded to EarthArvix which has not yet undergone peer review. It has been submitted for review. Subsequent versions may have different content.

Fast anisotropic Mg and H diffusion in wet forsterite

Joshua M R Muir[*1,3], Feiwu Zhang[1], Andrew M. Walker[2,3]

Corresponding author: Joshua M R Muir j.m.r.muir@mail.gyig.ac.cn

1) Institute of Geochemistry, Chinese Academy of Sciences, 99 West Lincheng Road, Guiyang, Guizhou 550081, China
2) Department of Earth Sciences, University of Oxford, South Parks Road, Oxford OX1 3AN, United Kingdom
3) Department of Earth Sciences, University of Leeds, Leeds, LS2 9JT, UK

Abstracts

Mg diffusion, which is important for properties of forsterite such as conductivity and deformation, is a strong function of water content. The mechanism behind this effect, however, has not been fully elucidated. In this study we use Density Functional Theory to predict the diffusivity of $(2H)^{X}_{Mg}$ and we find that they are around 1000 times slower than H-free Mg vacancies V''_{Mg}. In most wet conditions the concentration of $(2H)^{X}_{Mg}$ is much higher than that of V''_{Mg} and thus the primary effect of water on increasing the Mg-diffusion rate in forsterite is by producing large numbers of H-bearing Mg vacancies. A water induced increase in diffusion rate is predicted to be accompanied by a large increase in diffusional anisotropy primarily in the [001] direction. Using a previously developed model of H distribution in forsterite we predict that the effect of water on Mg diffusion is strongly dependent upon environmental conditions such as pressure or temperature. An exponent (r) describing

the relationship of water concentration to Mg diffusion is found to vary between 0.5-1.6 across common experimental conditions with pressure decreasing this exponent and temperature increasing it. With 100 wt. ppm water Mg diffusion rates are predicted to increase by over 2 orders of magnitude at high temperature and low pressure (2000 K, 0 GPa) and by over 3.5 orders of magnitude at low temperature and high pressure (1000 K, 10 GPa) while the anisotropy of diffusion is predicted to increase by ~2/over 5.5 orders of magnitude respectively. A conversion from "dry" to "wet" rheological laws is predicted to occur at <~1 ppm. These results suggest that Mg diffusion in wet forsterite could vary considerably throughout mantle conditions in ways that cannot be captured with a simple one component equation. Finally we considered the effects of the diffusion of H-bearing Mg vacancies on conductivity in forsterite and olivine. We combined our diffusivity results with experimentally determined results for phonon conductivity but this predicted significaly lower conductivities than have been observed experimentally in olivine, particularly at low temperatures (~1000 K). This suggests that the effect of water on olivine conductivity is not primarily due to bulk $(2H)_{Mg}^{X}$ diffusion and operates via a different unknown mechanism.

Keywords: Forsterite; Mg Diffusion; Water; Hydrogen; DFT

1) Introduction

Diffusion of Mg in olivine is an important ontrol on electrical conductivity (Fei et al., 2018, Yoshino et al., 2009, Yoshino et al., 2017, Schock et al., 1989, Sun et al., 2019, Gardes et al., 2014) in the upper mantle and potentially on deformation (Jaoul (1990)),

grain growth (Jung and Karato, 2001) and texture development (Karato et al., 2008). For this reason Mg diffusion rates have been studied extensively (see for example discussions in Charkaborty, 2010 and Jollands *et al.* 2020).

An important control on this diffusion rate in the upper mantle will be water (Demouchy and Bolfan-Casanova, 2016). Adding a small amount of water (~100 ppm) in the form of OH^- groups incorporated within the olivine crystal has been found to significantly enhance Mg diffusion rates (Fei et al., 2018) at 1300 K and 8 GPa. Hydrous diffusion has been described with the equation: $D_{Mg} = D_0(C_{H_2O})^r \exp\left(-\frac{E_{act}}{RT}\right)$ with the effect of water described by an exponent r which has been found to be 1.2±0.2 for Mg tracer diffusion (Fei et al., 2018) and to be ~1 for Fe-Mg interdiffusion (Wang et al., 2004). However, this water exponent is difficult to constrain by experiment as diffusion increases with water content but decreases with pressure, which also increases water fugacity. The mechanism by which water changes the diffusion rate is still unclear and experimental points are limited.

Thus in this work we shall use Density Functional Theory (DFT) to examine a possible mechanism by which water affects Mg diffusion, the production and diffusion of H-bearing Mg vacancies, and then calculate how varying conditions across pressure, temperature and composition space would affect this mechanism.

2 Methods

Diffusion is very slow compared to the timescales of atomistic simulations. To account for this we use a hybrid kinetic Monte Carlo (KMC) approach which is outlined in detail in Muir et al. (Submitted-a). In short, we first define the diffusing species

(Vac''_{Mg}, $Mg^{\bullet\bullet}_{Int}$, $(2H)^{X}_{Mg}$ all listed with Kroger-Vink notation) and determine their concentrations and the positions they can occupy in an olivine crystal lattice using density functional theory (DFT) and lattice dynamics within the quasi-harmonic approximation framework (QHA). The method for this is explored in Muir et al. (Submitted-b) as are the concentrations we use in this study. Second we determine all the possible "hops" between the different positions the defects can occupy and probe the energy landscape along these hops. This provides an energy barrier that each hop must overcome and the frequency at which this hop is attempted. Third, we combine information about multiple hops between different ground states using a kinetic Monte Carlo approach to access timescales long enough to observe the random walk and measure Mg diffusion in forsterite.

2.1 Diffusion Hops

To calculate diffusion coefficients we use a method fully outlined in Muir et al. (Submitted-a). In this work diffusion coefficients for Vac''_{Mg} and $Mg^{\bullet\bullet}_{Int}$ were calculated and the same method was used to calculate their coefficients in this work. In this work we also consider the diffusion of $(2H)^{X}_{Mg}$. As with Vac''_{Mg} in Muir et al. (Submitted-a) we define the movement of this defect as a series of hops (the same hops as for Vac''_{Mg} in Muir et al. (Submitted-a)). For each hop we calculate the activation energy by constructing a pathway along the hop and moving a Mg atom along this pathway. At each point the Mg atom is constrained to the path and the highest energy of the path (the transition state) is found. Diffusing $(2H)^{X}_{Mg}$ is more complex

than diffusing Vac''_{Mg} due to the presence of the hydrogen atoms. When determining the energy of the transition state for hydrous vacancies we assumed that hydrogen mobility is much higher than magnesium mobility (Novella et al., 2017) and so the hydrogen atoms follow the vacancy adiabatically. The procedure followed for hydrous vacancies is that described above (moving a Mg atom along the pathway and constrained to the pathway) but with hydrogen placed in a range of different positions (and relaxed without constraints) for each image. Hydrogen ions were placed in the MO_6 octahedron at the start or end of the path leading to four configurations for each image. One of these has two hydrogen atoms in the "start" octahedron, one has two hydrogen atoms in the "end" octahedron and two configurations have one hydrogen in each octahedron. Each point of the path then has four energies and at each point the lowest energy is selected to construct the path and find the transition state. This procedure assumes that throughout the process of magnesium diffusion the hydrogen atoms can rearrange to minimise the energy. We also attempted placing H outside the two MO_6 octahedra, but this gave higher energies than the previous configurations. In this way our activation energies for diffusion in hydrous forsterite are the minimum possible barriers as they ignore any barriers to hydrogen migration. Unless the energy of these hydrogen mobility barriers are close to the barriers of Mg migration they will be unimportant to the final rate of diffusion as diffusion rates are generally controlled by the rate of their slowest step. Once the transition state is determined we calculate its phonons using lattice dynamics and QHA and find the attempt frequency of the hop

using Vineyard theory as described in Muir et al. (Submitted-a). The rate of each hop is then determined with:

$$k = v^* exp\left(-\frac{H_m}{k_B T}\right)$$ Equation 1

Where v* is the attempt frequency from Vineyard theory and H_m is the activation energy. All the possible hop rates are then entered into our KMC model (Muir et al., Submitted-a) and a diffusion coefficient determined. Diffusion coefficients were calculated at 0, 5, 10 and 15 GPa and at 1000, 1500 and 2000 K.

2.2 Diffusion

Diffusion is then calculated with:

$$D_{Mg}^{sd} = D_{Mg}^{Vac} N_{Vac} + D_{Mg}^{Int} N_{Int} + D_{Mg}^{HVac} N_{HVac}$$ Equation 2

where D_{Mg}^{HVac} is the self diffusion coefficient for $(2H)_{Mg}^{X}$ as determined from KMC and N_{HVac} is the concentration of $(2H)_{Mg}^{X}$ using the method and values from Muir et al. (Submitted-b).

2.3 Pressure Correction

While DFT generally reliably reproduces pressure derivatives, the absolute pressures calculated by DFT are known to be systematically incorrect in that they are shifted in one direction. To correct for these we used a simple linear correction

$$P(V,T) = P^{DFT}(V,T) - P^{DFT}(V_0^{exp})$$ Equation 3

Where the subscript 0 represents the value of a parameter at a reference volume. For this equation we used V_0^{exp} values of 287.4 Å^3 for olivine (Isaak et al., 1989), 74.71 Å for MgO (Speziale et al., 2001) and 832.918 Å^3 for enstatite (Kung et al., 2004). This provided corrections of -4.95, -4.45 and -3.91 GPa respectively. The energy of

our reactions were then adjusted to account for these different pressure corrections using our calculated dE/dP values as were the diffusion coefficients. All pressures are presented corrected unless stated.

2.4 Units

Water in this paper shall refer to H-bearing defects. Concentrations shall be given as $[H_2O]_{bulk}$. This is the sum of the concentrations of all H-bearing defects with the concentrations of each defect normalised to contain the same amount of hydrogen as water. These are given in wt. ppm (1 wt. ppm=15.6 H/Si 10^6). Concentrations of Ti are given as wt. ppm TiO_2. "Pure" forsterite in this paper refers to a forsterite with no other defects (such as Ti) except H-bearing defects in the presence of water.

3 Results

3.1 Diffusion Coefficients of Hydrous Defects

Our calculated diffusion coefficients of V''_{Mg}, $Mg_I^{\bullet\bullet}$ and $(2H)^X_{Mg}$ are presented in Table 1. Discussion of the diffusivity of V''_{Mg} and $Mg_I^{\bullet\bullet}$ and more values are given in Muir et al. (Submitted-a).

We find that $(2H)^X_{Mg}$ has similar diffusive properties to V''_{Mg} but is around 1-3 orders of magnitude slower. With increasing pressure or temperature, the diffusivity of $(2H)^X_{Mg}$ approaches that of V''_{Mg}. Like V''_{Mg} (Muir et al., Submitted-a) the most favoured diffusion is overwhelmingly the "A" hop which is a hop between two adjacent M1 sites directly along the [001] chain of Mg atoms. This leads to highly anisotropic diffusion with diffusion along the [001] direction being orders of magnitude faster than

diffusion along the [010] or [100] directions. This anisotropy is much larger at lower temperatures because diffusion rates depend upon an exponential function of temperature ($e^{-\frac{E_a}{k_b T}}$). Increasing the pressure increases this anisotropy but to a much smaller degree than lowering temperature.

To examine the accuracy of our calculation we can compare our diffusivity with that obtained experimentally for hydrogen in forsterite. In iron-free systems the diffusion of hydrogen is expected to be controlled largely by $(2H)_{Mg}^{X}$ diffusion as it is the fastest diffusing hydrogen species (Padron-Navarta et al., 2014). Measuring this diffusion is complicated by the fact that the distribution of hydrogen can vary in different conditions and during diffusional processes different H-bearing defects can convert into one another. This was examined in Jollands (Submitted) where a combined distribution and diffusion model for hydrogen in forsterite was built. In this paper they determined that $(2H)_{Mg}^{X}$ diffusivity was at least an order of magnitude higher than previously measured (generally by fitting to Fick's second law) as $(2H)_{Mg}^{X}$ undergoes conversions to different H-bearing defects which slows the apparent rate when simply measuring concentration profiles. In Figure 1 we show a comparison between our calculated diffusivities and those determined from the model in Jollands (Submitted) and find strong agreement. We do not agree with previously measured diffusivities such as in Sun et al. (2019) that are around an order of magnitude of lower and were determined directly from fitting Fick's law for the reasons stated above. Some differences are expected as the experimental model includes all methods of hydrogen diffusion whereas we only consider $(2H)_{Mg}^{X}$ but the strong match between our

calculated data and the model fit to experiments in Jollands (Submitted) suggests both that $(2H)_{Mg}^{X}$ diffusivity largely controls hydrogen diffusivity in real forsterite and that our calculations accurately calculate its diffusivity.

3.2 Diffusion rates

To solve Equation 2 we need the diffusivities of various species (section 3.1) and their concentration. Calculating the relative concentration of H-bearing and H-free defects in forsterite is very complex and thus we built a model to do this as outlined in Muir et al. (Submitted-b). In that work we predicted that the main sites for water in forsterite are $(2H)_{Mg}^{X}$, $(4H)_{Si}^{X}$ and $\left\{\mathrm{Ti}_{\mathrm{Mg}}^{\bullet\bullet}(\mathrm{2H})_{\mathrm{Si}}^{''}\right\}^{\times}$. Of these defects $(4H)_{Si}^{X}$ has no straightforward effect on Mg diffusion and $\left\{\mathrm{Ti}_{\mathrm{Mg}}^{\bullet\bullet}(\mathrm{2H})_{\mathrm{Si}}^{''}\right\}^{\times}$ is likely immobile. Jollands (Submitted) concluded $\left\{\mathrm{Ti}_{\mathrm{Mg}}^{\bullet\bullet}(\mathrm{2H})_{\mathrm{Si}}^{''}\right\}^{\times}$ was immobile based on monitoring hydrogen diffusion rates in Ti-bearing forsterite. We calculated the binding energy of the two components of $\left\{\mathrm{Ti}_{\mathrm{Mg}}^{\bullet\bullet}(\mathrm{2H})_{\mathrm{Si}}^{''}\right\}^{\times}$ and found that it is high (~5-6 eV across upper mantle conditions depending upon pressure and temperature). To diffuse this cluster it would at some point have to overcome this energy barrier. A barrier of 5-6 eV can be compared to the lowest energy barriers that $(2H)_{Mg}^{X}$ needs to overcome to diffuse which are around 1.2 eV (Table S1). This means that the diffusion of $\left\{\mathrm{Ti}_{\mathrm{Mg}}^{\bullet\bullet}(\mathrm{2H})_{\mathrm{Si}}^{''}\right\}^{\times}$ will be many orders of magnitude slower than the diffusion of $(2H)_{Mg}^{X}$. Thus the important factor in wet Mg diffusion is $[(2H)_{Mg}^{X}]$.

Our predicted concentrations of defects are listed in Table 2. As was found in Muir et al. (Submitted-b) $(2H)_{Mg}^{X}$ is favoured at high temperatures, low pressures and low

water concentrations and thus Mg diffusion will be faster at these conditions. Free interstitial $H_i^{\bullet}$ is relatively favoured by low water concentrations and higher temperatures but its concentration is always predicted to be extremely low. $[Mg_I^{\bullet\bullet}]$ is suppressed by the addition of more water while $[V_{Mg}'']$ can both increase and decrease with the addition of water due to reactions such as the production of $(4H)_{Si}^{X}$ which also produces V_{Mg}''. In all cases H-bearing defects greatly outnumber H-free defects. Our predicted diffusion rates as a function of water are shown in Figure 2 and with a comparison to the experimental values of Fei et al. (2018) in Figure 3. In general there is initially a very sharp increase in diffusion with increasing amounts of water- conversion from a "dry" to a "wet" regime- and then a slower increase in diffusion with increasing water- the "wet" regime. In the "dry" regime $[V_{Mg}'']$ is much larger than $[(2H)_{Mg}^{X}]$ or they have similar values. In the "wet" regime $[(2H)_{Mg}^{X}]$ is much larger than $[V_{Mg}'']$.

For the comparisons to the values of Fei et al. (2018) in Figure 3 we present both "pure" forsterite and forsterite with 80 wt. ppm TiO_2, as TiO_2 is one of the impurities present in the experiments of Fei et al. (2018) and one which could affect wet diffusion by allowing the formation of immobile $\left\{\mathrm{Ti}_{\mathrm{Mg}}^{\bullet\bullet}(2\mathrm{H})_{\mathrm{Si}}^{''}\right\}^{\times}$. We find that Ti can cause a difference in diffusion rates at low pressures, low temperatures and low water concentrations through the formation of $\left\{\mathrm{Ti}_{\mathrm{Mg}}^{\bullet\bullet}(2\mathrm{H})_{\mathrm{Si}}^{''}\right\}^{\times}$ over $(2H)_{Mg}^{X}$ but that at the conditions used in Fei et al. (2018) Ti-free and Ti-containing samples largely have identical traces because $(4H)_{Si}^{X}$ is favoured over both $\left\{\mathrm{Ti}_{\mathrm{Mg}}^{\bullet\bullet}(2\mathrm{H})_{\mathrm{Si}}^{''}\right\}^{\times}$ and $(2H)_{Mg}^{X}$. We find a good match between our values and those of Fei et al. (2018) at higher water

contents but an increasing mismatch with lower water contents. This is unsurprising as when we consider the high pressures conditions of the experiments where we predict that water is overwhelmingly in $(4H)_{Si}^{X}$ defects. We predict that at these conditions water in $(2H)_{Mg}^{X}$ defects makes up between 0.01-0.2% of the total water content (with this number decreasing with increasing $[H_2O]_{bulk}$) which is also observed by the lack of an identifiable $(2H)_{Mg}^{X}$ peak in the FTIR signal presented in Fei et al. (2018). Thus very small errors in determining the total water content, the pressure or the temperature would lead to large errors in relative $[(2H)_{Mg}^{X}]$ concentration which becomes increasingly more important as water concentration decreases. Kinetics could also be an issue in the experiment. We predict that most water in forsterite in high pressure conditions resides in $(4H)_{Si}^{X}$ defects. The production of $(4H)_{Si}^{X}$ reduces Mg diffusion rates by reducing $[(2H)_{Mg}^{X}]$. We predict, however, that the production of $(4H)_{Si}^{X}$ occurs through a reaction involving the interaction of 2 $(2H)_{Mg}^{X}$ defects and thus its rate is also dependant on Mg diffusion rates. Thus the distribution and the diffusion of $(2H)_{Mg}^{X}$ likely operate on similar timescales though this should be less of an issue at the long time scales of the mantle where thermodynamic equilibration is likely. Experiments done at high pressure and low temperatures should be less impacted by such concerns as a larger proportion of the water is taken up by $(2H)_{Mg}^{X}$ defects in these conditions.

We fit an equation to plot the effect of water on the diffusion rate:

$$D_{sd} = a + [H_2O]_{bulk}^{r} * b \quad \text{Equation 4}$$

where a, b and r are fitting variables. The results are shown in Table 3 (anisotropy and Ti-free values) and Table 4 (Ti-bearing values). We did this separately for the "dry" and the "wet" regime. The $[H_2O]_{bulk}$ value at which the "wet" region begins is tabulated in Table 3 and for "pure" forsterite is always below 1 wt. ppm. Thus at realistic concentrations of water only the "wet" region is important for Mg diffusion and these are the values presented in Table 3.

First we shall consider the value of r which is the key variable in how changing the concentration of water changes diffusion rates. r varies strongly with condition going from 0.55 at high pressure and low temperature to 0.88 at high temperature and low temperature in "pure" forsterite. In general increasing pressure decreases r and increasing temperature increases r. In the presence of Ti (Table 4) r has even more possible variations with increasing Ti leading to large increases in r particularly at low temperatures. Thus r is highly dependent upon experimental condition and no one fitting of Equation 4 or similar equations can capture the effect of water on Mg diffusion rates across mantle relevant temperatures, pressures and compositions.

To understand why this is the case we must consider how varying $[H_2O]_{bulk}$ varies the diffusion rate. In the wet region where $[(2H)_{Mg}^{X}] >> [V_{Mg}'']$ the diffusion rate increases with increasing $[H_2O]_{bulk}$ overwhelmingly because $[(2H)_{Mg}^{X}]$ increases. The rate of increase of the Mg diffusion rate is thus proportion to how $[(2H)_{Mg}^{X}]$ varies with $[H_2O]_{bulk}$:

$$[(2H)_{Mg}^{X}] \propto [H_2O]_{bulk}^{rc} \quad \text{Equation 5}$$

with rc in Equation 5 being very similar to r in Equation 4. The variation of rc values with condition are explored in detail in Muir et al. (Submitted-b) but in short rc values are heavily dependant on which H-bearing defects are dominant at any specific condition. In a heavily $(4H)_{Si}^{X}$ dominated system (such as at low temperature and high pressures) rc in Equation 5 is ½ and thus r in Equation 4 should approach 0.5. In a heavily $(2H)_{Mg}^{X}$ dominated system (such as at high temperature and low pressures) rc in Equation 5 is 1 and thus r in Equation 4 should approach 1. The presence of Ti causes complex variations in $[(2H)_{Mg}^{X}]$ and thus allows a varied range of r values that are larger than in Ti-free cases. In the absence of Ti it is difficult for r to be above 1 as it would require the dominant charge carrier to have less than 2 hydrogen. In Muir et al. (Submitted-b) we demonstrate a situation where the concentration exponent for hydrous Mg vacancies is ~1.2 (due to the formation of $H_{Mg}^{\prime}$) but this is only possible in the presence of Al and at low pressures**.**

Fei et al. (2018) found an exponent r of ~1.2 at 1300 K and 8 GPa. We predict this exponent to be much lower (~0.6) even in the presence of Ti. Our distribution model predicts that at these conditions most water would be in $(4H)_{Si}^{X}$ which also appears to be the case from the IR spectra in Fei et al. (2018) which shows a large peak at ~3610 and some bands between 3450-3600 cm-1 which are generally attributed as $(4H)_{Si}^{X}$ bands (Tollan et al., 2017). When $(4H)_{Si}^{X}$ is the dominant H-bearing defect it is extremely difficult for the water diffusion exponent r to rise above 1 as this would generally require the relevant diffusing species to have more than 4 H atoms in its structure. Even if $(4H)_{Si}^{X}$ diffusion contributes significantly to Mg diffusion rates

289 then r would be close to but below 1. An r value of 1.2 is an indication either that
290 some much more complicated mechanism is happening than we have modelled here or
291 that the fitting of the exponent is extremely sensitive. Our ability to generally replicate
292 the diffusion values of Fei et al. (2018) (Figure 3) suggests the latter case is true.
293 Outside of the exponent the difference between the base diffusion rates of "dry" and
294 "wet" forsterite (a in Equation 4) vary with pressure and temperature. In dry
295 forsterite temperature increases the diffusion rate markedly (due to the $e^{(-\frac{\Delta H}{k_b T})}$ term in
296 determing diffusivity and the increased concentration of intrinsic defects) whereas
297 pressure decreases it slightly (mostly due to lower number of intrinsic defects being
298 produced). For wet diffusion increasing the temperature increases $[(2H)_{Mg}^{X}]$ and
299 diffusivity and thus diffusion rates while increasing the pressure decreases $[(2H)_{Mg}^{X}]$
300 and thus diffusion rates sharply (Table 2). These trends can be seen in Table 3 or
301 Figure 2.
302 Outside of pressure and temperature other factors are important to wet Mg diffusion
303 rates. The choice of buffer will have a strong effect as increasing $aSiO_2$ increases the
304 favourability of $(2H)_{Mg}^{X}$ and thus increases the effect of water on Mg diffusion rates.
305 This is plotted in Figure S1 where we find in some case multiple orders of magnitude
306 difference between diffusion rates in an MgO or an $MgSiO_3$ buffered system with MgO
307 buffered systems have considerably slower diffusion rates. This is a useful test of the
308 predictions of our model as the predicted differences are large. All results in this work
309 shall be presented with an $MgSiO_3$ buffer as it is closer to the conditions of the mantle.

Ti is present in the study of Fei et al. (2018) and can be an important defect as it can decrease the formation of $(2H)_{Mg}^{X}$ in favor of immobile $\left\{\mathrm{Ti}_{\mathrm{Mg}}^{\bullet\bullet}(\mathrm{2H})_{\mathrm{Si}}^{''}\right\}^{\times}$. Table 4 plots the effect of Ti on Mg diffusion rates where we find that Ti has a large effect at low temperatures and pressures where $\left\{\mathrm{Ti}_{\mathrm{Mg}}^{\bullet\bullet}(\mathrm{2H})_{\mathrm{Si}}^{''}\right\}^{\times}$ is favoured but little effect on the Mg diffusion rate as temperature or pressure increases. Al allows the formation of H'_{Mg} (Muir et al., Submitted-b). This will speed up Mg diffusion as every 1 $(2H)_{Mg}^{X}$ can form 2 H'_{Mg} thus doubling the concentration of diffusing species. We do not know the diffusivity of H'_{Mg} but it is likely between that of $(2H)_{Mg}^{X}$ and V''_{Mg} which will further speed up diffusion as $(2H)_{Mg}^{X}$ defects diffuse a lot slower than a V''_{Mg} defect.

Thus we conclude that while water generally increases Mg diffusion rates the exact amount which it increases and the dependence of this increase on water concentration is highly dependent on the background conditions such as pressure and temperature and that extrapolating between these regimes is not straightforward. Thus when quantifying the effect of water on forsterite diffusion rates- and the rates of properties depedant upon diffusion- measurements need to be made at the conditions in which you are interested as extrapolating to these conditions is not straightforward.

3.3 Diffusional Anisotropy

As well as an increase in diffusion rate we also predict water to lead to a sharp increase in diffusional anisotropy. Anisotropy is shown for a sample composition in Figure 4 though all compositions have similar traces with the values explored in Table 3. At

low water contents in the "dry" diffusion regime diffusion and its anisotropy are controlled by V''_{Mg} and $Mg_I^{\bullet\bullet}$. At high water contents in the "wet" diffusion regime diffusion and its anisotropy is controlled primarily by $(2H)^X_{Mg}$. Inside each regime the anisotropy of diffusion comes from the anisotropy of the diffusion coefficients of V''_{Mg} and $Mg_I^{\bullet\bullet}$ or $(2H)^X_{Mg}$ and thus is sensitive to temperature and pressure but insensitive to water and Ti concentration. Increasing the temperature decreases the anisotropy, increasing the pressure increases it. As $(2H)^X_{Mg}$ has highly anisotropic diffusion favouring the [001] direction (Table 1) Mg diffusion in the wet region is highly anisotropic favouring the [001] direction. The anisotropy of diffusion is listed in Table 3 with wet forsterite possessing Mg diffusion that is 1-4 orders of magnitude more anisotropic than dry forsterite. We are not aware of any experimental measures of the anisotropy of Mg diffusion in wet forsterite but this would be a good test of our model as the effect is very large particularly at low temperatures.

4. Discussion

4.1 Diffusion Rates in Upper Mantle Conditions

The main conclusion of this work is that water increases the rate and the anisotropy of Mg diffusion in forsterite but that the magnitude of this effect is highly dependent upon the prevailing conditions. Thus we stress that the effect of water on Mg diffusion must be measured and constrained in the relevant conditions as extrapolation is extremely difficult. Even then it will be difficult to fit the effect of water to simple relationships across geophysically relevant P and T ranges.

To demonstrate this we projected our results along one relevant P and T range, an oceanic geotherm, with the results shown in Figure 5. We predict that water has a varied effect on Mg diffusion with depth. In the shallow upper mantle water causes a large (up to 4 orders of magnitude for 100 wt. ppm water) increase in diffusion rate which increases with depth before peaking at ~100 km. As depth increases the effect of water decreases until 410 km where even an extremely wet forsterite (1000 wt. ppm) has a Mg diffusion rate that is less than 1 order of magnitude higher than dry forsterite. This varying behaviour is due largely to variations in $[(2H)^{X}_{Mg}]$ which initially increases, peaks at 100 km then decrease sharply in favour of $[(4H)^{X}_{Si}]$. The presence of even large amounts of Ti decreases the maximum diffusion rate of wet forsterite but not to a large degree. The effect of $[H_2O]_{bulk}$ on Mg diffusion rates is thus varied, complex and changes with depth.

Water is predicted to also induce large differences in the anisotropy of Mg diffusion with "wet" forsterite generally being 2-3 orders of magnitude more anisotropic than dry samples (Figure 6). As discussed above anisotropy is insensitive to water content above a small value of $[(2H)^{X}_{Mg}]$ which is likely exceeded in wet samples in the upper mantle and thus all concentrations of water will lead to identical diffusional anisotropy. Our predicted anisotropy of Mg diffusion in Figure 6 has many peaks and features based on temperature and pressure variations which will vary significantly with thermal fluctuations but the effect of water in increasing anisotropy is robust up until the final ~10 km of the lower mantle where $[(2H)^{X}_{Mg}]$ concentrations are predicted to decrease sharply and so the anisotropy of diffusion is also predicted to decrease sharply.

The predicted anisotropy of wet forsterite is large and it is possible that real wet forsterite is not so anisotropic. For wet forsterite to be less anisotropic than predicted here some kind of macroscopic mechanism that reduces diffusional anisotropy likely needs to be present. We predict that the hopping of vacancies, both H-bearing and H-free, is highly anisotropic along the [001] direction. This makes sense when considering the structure of forsterite as there is an unobstructed diffusion path along the [001] chains of M1 Mg atoms whereas movement in any other direction involves obstructions of other atoms. The activation energy of this A-hop is low (~1 eV in H-free vacancies, ~1.2 eV in H-bearing defects) and any alternative diffusional mechanisms would need a similarly low activation energy if they were to compete with the A-hop and lower anisotropy. We have only considered simple one site hopping and it is possible there is some kind of conjoined multi-site hopping but this would be unlikely to have such a low activation energy. Our ability to replicate some experimentally measured dry (Muir et al., Submitted-a) and wet (Figure 3) diffusion parameters suggests our mechanism is mostly correct. Water could produce a defect that is not a vacancy but that also contributes to Mg diffusion but it is unclear what such a defect would be.

It is important to emphasise that these studies lack iron which would affect conclusions in olivine. The primary way this could happen is that iron could reduce the amount of $(2H)_{Mg}^{X}$ that is formed by allowing the formation of alternative hydrogen complexes. This will reduce the effect of water on Mg diffusion rates. The trends with pressure,

temperature, buffer activity and Ti concentration should all remain largely intact however unless iron-hydrogen complexes are strongly favoured in all conditions. The predicted increase in Mg diffusional anisotropy in particular is insensitive to the amount of water above a small value and thus unless Fe complexes drastically reduce the value of $[(2H)^{X}_{Mg}]$ we predict Mg diffusion in wet olivine to remain very anisotropic. Thus the trends seen in diffusion speed and anisotropy with depth in wet forsterite should remain in wet olivine and throughout upper mantle conditions water will affect diffusion rates differently and no one simple water effect will be present.

4.2 The effect of Mg diffusion rate variations on Conductivity

As an example of how these properties affect the upper mantle we calculated the properties of one key property that is controlled in part by Mg diffusion, conductivity. Previously the observed conductivity of olivine has been explained with a model that combines three major mechanisms: proton-polaron hopping, Mg vacancy hopping and some hydrous factor (Gardes et al., 2014). The exact nature of the hydrous factor is unknown with some work speculating it is due to $(2H)^{X}_{Mg}$diffusion (Fei et al., 2018). We thus built a model to examine whether our Mg diffusion rates could explain observed conductivity in olivine. We predicted conductivity via the following equation:

$$\sigma = \sigma_0^{Polaron} e^{-\frac{\Delta H^{Pol}}{RT}} + \frac{D^*_{vac}\times[V''_{Mg}]}{RT} \times (2 \times F)^2 + \frac{D^*_{int}\times[Mg^{\bullet\bullet}_I]}{RT} \times (2 \times F)^2 + \frac{D^*_{HMgVac}\times[(2H)^X_{Mg}]}{RT} \times (2 \times F)^2 + \frac{D^*_{HSivac}\times[(4H)^X_{Si}]}{RT} \times (4 \times F)^2 \quad \text{Equation 6}$$

with activation energies in kJ/mol, concentrations in mol/m^3 and F is the Faraday constant. The first term refers to proton-polaron hopping. We have not calculated this and have taken values for these terms directly from Gardes et al. (2014). The next 4 terms refer to the diffusion of Mg vacancies, Mg interstitials, $(2H)^X_{Mg}$ and $(4H)^X_{Si}$ respectively with conductivity calculated from the Nerst-Einstein equation. In the formulation of Gardes et al. (2014) there was no diffusion term for Mg interstitials but we find that Mg vacancies and Mg interstitials have similar diffusion rates in dry forsterite and thus this term should be included. The parameters for all diffusion terms were taken from this work except for the diffusivity of $(4H)^X_{Si}$ which we have not calculated. Diffusivity was set to $D^*_{HSivac} = 10^{3.3}\exp\left[-\frac{461}{RT}\right]$ taken from Padron-Navarta et al. (2014). This equation lacks a pressure derivative and likely represents some combination of inherent $(4H)^X_{Si}$ diffusivity and the rate of $(4H)^X_{Si}$ converting to $(2H)^X_{Mg}$, diffusing and then converting back but this is not a major component of the conductivity (see M3 vs M4 in Figure S2) and thus the exact diffusivity of $(4H)^X_{Si}$ doesn't change our overall conclusion. We have neglected the diffusion of Si and O vacancies in our model as their concentrations are predicted to be very small (<1x10^{-15} defects/fu) and thus irrelevant when considering the effects of water. Any $\left\{\mathrm{Ti}^{\bullet\bullet}_{\mathrm{Mg}}(\mathrm{2H})^{''}_{\mathrm{Si}}\right\}^{\times}$ that is produced was considered immobile and thus non-conductive for the reasons discussed above.

$(2H)^X_{Mg}$ and $(4H)^X_{Si}$ present a problem as formally these species do not carry a charge and thus their diffusion does not contribute to conductivity. As argued by Fei et al. (2018) if there is exchange between$(2H)^X_{Mg}$and V''_{Mg} then the diffusion of $(2H)^X_{Mg}$

contributes to the movement of charge carriers and thus conductivity and an identical argument could be made about $(4H)_{Si}^{X}$ and V_{Si}''''. Such a mechanism would introduce an extra step to the "diffusion of charge carriers" and the exchange rate between $(2H)_{Mg}^{X}$and V_{Mg}'' would be important in this scenario. We have assumed that this exchange step is very fast and that the rate limiting step is the diffusion of $(2H)_{Mg}^{X}$and/or V_{Mg}'' and thus any exchange kinetics can be ignored. This may not be accurate but in this way we have assumed the maximum conductivity from this mechanism as any exchange kinetics will effectively slow down the diffusion of charge carriers and thus reduce conductivity. As will be seen even with this assumption (and other assumptions that maximise conductivity such as ignoring the effect of iron as discussed below) our predicted conductivity is too small rather than too large.

In Figure 7 (with a 2D plot of conductivity in Figure S3) we plot our predicted conductivity vs those determined from the model in Gardes et al. (2014) (G14)**.** The G14 model correctly replicates a range of experimental observations and thus a model that matches G14 also matches experimental observations. The most important fact is that our model predicts very different conductivities from G14 and generally lower conductivities even though our model likely overpredicts conductivity as discussed above**.** This misfit is largest at low temperatures where proton-polaron conductivity should be dominant. This is a curious result as our proton-polaron numbers are taken directly from G14 and so it would be expected that our fitting would be better at low temperature and worse at high temperature where we find some weak agreement between our model and G14**.** A further problem comes when you consider different

463 water concentrations- the misfit between our model and that of G14 is highly variable
464 and depends upon $[H_2O]_{bulk}$. This strongly suggests our model does not correctly
465 represent how water affects olivine conductivity as a correct mechanism should scale
466 with $[H_2O]_{bulk}$ in a way that replicates experimental observations which are matched by
467 the model of G14.
468 There are many other inconsistencies between our model and that of G14**.** As shown
469 in Figure 8 our predicted anisotropy of conduction is opposite to that of G14 even at
470 high temperatures where a diffusion mechanism, which favours [001] conduction,
471 would be predicted to be strong. The preservation of conductivity favouring an [010]
472 anisotropy even at high temperatures in the G14 model is evidence that something other
473 than a diffusive vacancy mechanism is important in wet olivine conduction.
474 In Table 5 we compare activation energies for the hydration part of G14 with those
475 predicted in our model. Our activation energies are considerably higher. It is
476 important to clarify the term "activation energy". In a diffusion mechanism there are
477 at least 2 activation energies- one for hopping of the defects (Table S1**)** and one for
478 production of the defects (Table 2)- and in a hydrated system where the concentration
479 and mobility of $(2H)_{Mg}^{X}$ are both strong functions of temperature both of these are
480 important. If ionic diffusion is important to olivine conductivity at least 2 activation
481 energies are likely required to model the effect of water. In experimental fittings of
482 diffusion or conductivity with temperature these two features will be combined into a
483 single "activation energy" which we have done in Table 5 with the first four columns
484 showing a "normal" activation energy containing two parts and the final column

485 showing an activation energy with a fixed $(2H)_{Mg}^{X}$ concentration thus removing the
486 production of defects component. In either case our predicted activation energy is
487 much higher than that of G14.
488 The water concentration exponent "r" is also different between our model and G14.
489 In the case of conductivity being proportional to $(2H)_{Mg}^{X}$ diffusion then r should be
490 equal to that for Mg diffusion in Table 3. Gardes et al. (2014) found two good fits
491 with the favoured one having r=1/3 and the less favoured one r=1.99. Neither of these
492 fit either our r value in Table 3 or r values that can be easily achieved when considering
493 mechanisms for producing $(2H)_{Mg}^{X}$. If $(4H)_{Si}^{X}$ is considered to be the controlling
494 species for conductivity then r=2 in some cases (Kohlstedt, 2006, Muir et al.,
495 Submitted-b) but this is difficult to rectify with the slow diffusion rate of $(4H)_{Si}^{X}$
496 (Padron-Navarta et al., 2014) even if it is the dominant water species. Finally in
497 Figure S2 we add/remove different parts to Equation 6 and consider the case of H'_{Mg}
498 produced by Al to examine how each part of Equation 6 modifies the final conductivity
499 but in no case do we find anything that closely matches the G14 model.
500 The very different behaviour predicted by our model compared to that of Gardes et al.
501 (2014), which matches experimental observations, is evidence that our model is
502 incorrect. This is perhaps unsurprising as our model relies upon the diffusion of
503 $(2H)_{Mg}^{X}$ and $(4H)_{Si}^{X}$ which are formally not charge carriers. Previously it has been
504 suggested that water produces interstitial hydrogen ($H_i^{\bullet}$) which is a charge carrier and
505 that it is the diffusion of $H_i^{\bullet}$ that explains the conductivity (Sun et al., 2019, Karato,
506 2013). As shown in Table 3 and discussed more in Muir et al. (Submitted-b) our

calculations predict that $H_i^{\bullet}$ is unlikely to form in significant concentrations particularly at high water concentrations. A further argument against $H_i^{\bullet}$ diffusion being the important factor is that our mismatch with G14 is highest at low temperatures. $H_i^{\bullet}$ is favoured by high temperatures because it has more configurational entropy than other H-bearing defects. Thus if our model simply missed a $H_i^{\bullet}$ diffusion factor we would expect better matches to G14 at low temperature and worse matches at high temperatures. Measurements of $H_i^{\bullet}$ diffusion rates also lead to higher activation energies and anisotropy than is seen in G14 (Kohlstedt and Mackwell, 1998).

In Figure 8 we compare our results to another model, that of Fei et al. (2020). This model was constructed from high temperature measures of conductivity and thus was designed to more accurately capture the high temperature mechanism of conductivity which is expected to be ionic conduction. The activation energy of the water mechanism in this work was found to be 337 kJ/mol along the [100] direction, 396 along the [010] and 385 along the [001]. These are generally higher than the values we found in Table 5, the opposite problem with the comparison to G14. As can be seen in Figure 8 the model of Fei et al. (2020) produces anisotropies in the same order ([001]>[010]>[100]) as in our work but with extremely different temperature dependence that doesn't fit our predictions at all.

In this work we have not calculated the effect of iron. We include the effect of polarons which arise from iron but through the fitting from Gardes et al. (2014). Iron will have some effect on V''_{Mg} through Mg-Fe interdiffusion effects but the overall rate of Mg self and Mg-Fe interdiffusion is similar (Chakraborty, 2010) and thus is not an

explanation for the conductivity differences here. Fe can allow the formation of trivalent compounds with water, likely $\{Fe^{\bullet}_{Mg}H'_{Mg}\}^{\times}$ (Berry et al., 2007). This defect contains two charge carriers $Fe^{\bullet}_{Mg}$ and H'_{Mg} but we calculate the binding energy to be 2.3-2.8 eV at 1500 K and from 0-10 GPa and thus these carriers are strongly bound to each other and unlikely to diffuse. The formation of $\{Fe^{\bullet}_{Mg}H'_{Mg}\}^{\times}$ will reduce the concentration of $(2H)^{X}_{Mg}$ and $(4H)^{X}_{Si}$ and thus further reduce conductivity and increase the mismatch between our diffusive model and reality. Experimental evidence also suggests that Fe-hydrogen complexes are unlikely contributors to conductivity. These complexes are expected to involve ferric iron and thus if they contributed strongly to conductivity, conductivity would be expected to increase with increasing oxygen fugacity which converts ferrous iron to ferric iron and thus would be expected to increase the concentration of ferric-hydrogen complexes. In Dai and Karato (2014)**,** however, it was found that conductivity is inversely proportional to oxygen fugacity. This relationship suggests that ferrous iron is a stronger contributor to conductivity than ferric iron. Thus the presence of iron should not explain the discrepancies found here.

Similar to iron the presence of Ti can form $\{Ti^{\bullet\bullet}_{Mg}(2H)^{''}_{Si}\}^{\times}$ which is likely immobile. This will reduce of the concentration of $(2H)^{X}_{Mg}$ and $(4H)^{X}_{Si}$ (Muir et al., Submitted-b) and thus the conductivity even further. This is in contrast to measurements by Dai and Karato (2020) where it was found that Ti increases conductivity in water poor regions where $\{Ti^{\bullet\bullet}_{Mg}(2H)^{''}_{Si}\}^{\times}$ is important and has little effect in water rich regions where $\{Ti^{\bullet\bullet}_{Mg}(2H)^{''}_{Si}\}^{\times}$ is unimportant. For Ti to increase conductivity in an ionic

regime $\left\{\mathrm{Ti}_{\mathrm{Mg}}^{\bullet\bullet}(2\mathrm{H})_{\mathrm{Si}}^{''}\right\}^{\times}$ would have to diffuse quickly which we find to be unlikely so this is further evidence that the mechanism by which water increases conduction in olivine is not ionic diffusion.

All of these problems combined means that is very unlikely that the contribution of water to olivine conductivity is through bulk $(2H)_{Mg}^{X}$ or $(4H)_{Si}^{X}$ diffusion. A more likely explanation is that water has an electronic effect on conductivity through adding donor or acceptor states to the bandgaps as has been seen in oxide semiconductors (McCluskey et al., 2012) or alternatively water could affect grain boundary diffusion which could be important in olivine conductivity (Han et al., 2021). As our model increasingly diverges from that of G14 as temperature decreases either the new mechanism for the effect of water on conductivity must be strong at low temperatures or the polaron mechanism must be stronger than is predicted in G14 and the water mechanism weaker.

5. Conclusion:

In conclusion we predict that water increases both the Mg diffusion rate of forsterite and the anisotropy significantly with these increases being over 2/5 orders of magnitude in the right conditions. The increase in diffusion rate is proportional to the water concentration while the increase in anisotropy does not depend on the concentration except at very low water concentrations (<~1 wt. ppm). These effects are large and should be visible in experiments.

We predict that both the magnitude of the increase in Mg diffusion rates and the exponent that governs how they change with water concentration vary strongly depending upon environmental conditions. This is because they are related to the concentration of $(2H)_{Mg}^{X}$ which also has strong condition dependence. Notably increasing the pressure decreases the effect of water on diffusion as it promotes $(4H)_{Si}^{X}$ over $(2H)_{Mg}^{X}$. We showed the effect of this complexity by plotting Mg diffusion in wet along a geotherm and find that in wet forsterite it peaks around 100 km in an oceanic geotherm with sharp decreases in diffusion rate on either side of this depth. This demonstrates that Mg diffusion rates in wet forsterite cannot be modelled with one simple parameter and that the full system of water distribution and $(2H)_{Mg}^{X}$ diffusion rates need to be taken into account to model Mg diffusion. Finally we consider the effect of our predictions on wet conductivity rates in olivine and find very large differences between our predicted conductivities and those observed in olivine suggesting that the effect of water on olivine conductivity is not through ionic diffusion.

BERRY, A. J., O'NEILL, H. S. C., HERMANN, J. & SCOTT, D. R. 2007. The infrared signature of water associated with trivalent cations in olivine. *Earth and Planetary Science Letters,* 261**,** 134-142.

CHAKRABORTY, S. 2010. Diffusion Coefficients in Olivine, Wadsleyite and Ringwoodite. *In:* ZHANG, Y. X. & CHERNIAK, D. J. (eds.) *Diffusion in Minerals and Melts.*

DAI, L. & KARATO, S.-I. 2014. Influence of oxygen fugacity on the electrical conductivity of hydrous olivine: Implications for the mechanism of conduction. *Physics of the Earth and Planetary Interiors,* 232**,** 57-60.

598 DAI, L. & KARATO, S.-I. 2020. Electrical Conductivity of Ti-Bearing Hydrous Olivine
599 Aggregates at High Temperature and High Pressure. *Journal of Geophysical*
600 *Research-Solid Earth,* 125.
601 DEMOUCHY, S. & BOLFAN-CASANOVA, N. 2016. Distribution and transport of hydrogen
602 in the lithospheric mantle: A review. *Lithos,* 240**,** 402-425.
603 FEI, H., DRUZHBIN, D. & KATSURA, T. 2020. The Effect of Water on Ionic Conductivity in
604 Olivine. *Journal of Geophysical Research-Solid Earth,* 125.
605 FEI, H. Z., KOIZUMI, S., SAKAMOTO, N., HASHIGUCHI, M., YURIMOTO, H., MARQUARDT,
606 K., MIYAJIMA, N. & KATSURA, T. 2018. Mg lattice diffusion in iron-free olivine and
607 implications to conductivity anomaly in the oceanic asthenosphere. *Earth and*
608 *Planetary Science Letters,* 484**,** 204-212.
609 GARDES, E., GAILLARD, F. & TARITS, P. 2014. Toward a unified hydrous olivine electrical
610 conductivity law. *Geochemistry Geophysics Geosystems,* 15**,** 4984-5000.
611 HAN, K., GUO, X. Z., ZHANG, J. F., WANG, X. B. & CLARK, S. M. 2021. Fast grain-boundary
612 ionic conduction in multiphase aggregates as revealed by electrical conductivity
613 measurements. *Contributions to Mineralogy and Petrology,* 176.
614 ISAAK, D. G., ANDERSON, O. L., GOTO, T. & SUZUKI, I. 1989. ELASTICITY OF SINGLE-
615 CRYSTAL FORSTERITE MEASURED TO 1700-K. *Journal of Geophysical Research-*
616 *Solid Earth and Planets,* 94**,** 5895-5906.
617 JAOUL, O. 1990. MULTICOMPONENT DIFFUSION AND CREEP IN OLIVINE. *Journal of*
618 *Geophysical Research-Solid Earth and Planets,* 95**,** 17631-17642.
619 JOLLANDS, M. Submitted. Hydrogen diffusion in olivine: the effect of inter-site reactions.
620 JOLLANDS, M. C., ZHUKOVA, I. A., O'NEILL, H. S. & HERMANN, J. 2020. Mg diffusion in
621 forsterite from 1250-1600 °C. *American Mineralogist***,** DOI: 10.2138/am-2020-
622 7286.
623 JUNG, H. & KARATO, S. I. 2001. Effects of water on dynamically recrystallized grain-size
624 of olivine. *Journal of Structural Geology,* 23**,** 1337-1344.
625 KARATO, S.-I. 2013. Theory of isotope diffusion in a material with multiple species and its
626 implications for hydrogen-enhanced electrical conductivity in olivine. *Physics of*
627 *the Earth and Planetary Interiors,* 219**,** 49-54.
628 KARATO, S., JUNG, H., KATAYAMA, I. & SKEMER, P. 2008. Geodynamic significance of
629 seismic anisotropy of the upper mantle: New insights from laboratory studies.
630 *Annual Review of Earth and Planetary Sciences.*
631 KOHLSTEDT, D. L. 2006. The role of water in high-temperature rock deformation. *In:*
632 KEPPLER, H. & SMYTH, J. R. (eds.) *Water in Nominally Anhydrous Minerals.*
633 Chantilly: Mineralogical Soc Amer & Geochemical Soc.
634 KOHLSTEDT, D. L. & MACKWELL, S. J. 1998. Diffusion of hydrogen and intrinsic point
635 defects in olivine. *Zeitschrift Fur Physikalische Chemie-International Journal of*
636 *Research in Physical Chemistry & Chemical Physics,* 207**,** 147-162.
637 KUNG, J., LI, B. S., UCHIDA, T., WANG, Y. B., NEUVILLE, D. & LIEBERMANN, R. C. 2004. In
638 situ measurements of sound velocities and densities across the orthopyroxene -
639 > high-pressure clinopyroxene transition in MgSiO3 at high pressure. *Physics of*
640 *the Earth and Planetary Interiors,* 147**,** 27-44.

MCCLUSKEY, M. D., TARUN, M. C. & TEKLEMICHAEL, S. T. 2012. Hydrogen in oxide semiconductors. *Journal of Materials Research,* 27**,** 2190-2198.

MUIR, J., ZHANG, F. & WALKER, A. M. Submitted-a. The Controls of Pressure and Water on Highly Anisotropic Mg Diffusion in Forsterite**.,** Preprint available at https://doi.org/10.31223/osf.io/ck3af.

MUIR, J. M. R., JOLLANDS, M., ZHANG, F. & WALKER, A. M. Submitted-b. Controls on the distribution of hydrous defects in forsterite from a thermodynamic model.

NOVELLA, D., JACOBSEN, B., WEBER, P. K., TYBURCZY, J. A., RYERSON, F. J. & DU FRANE, W. L. 2017. Hydrogen self-diffusion in single crystal olivine and electrical conductivity of the Earth's mantle. *Scientific Reports,* 7**,** 10.

PADRON-NAVARTA, J. A., HERMANN, J. & O'NEILL, H. S. C. 2014. Site-specific hydrogen diffusion rates in forsterite. *Earth and Planetary Science Letters,* 392**,** 100-112.

SCHOCK, R. N., DUBA, A. G. & SHANKLAND, T. J. 1989. ELECTRICAL-CONDUCTION IN OLIVINE. *Journal of Geophysical Research-Solid Earth and Planets,* 94**,** 5829-5839.

SPEZIALE, S., ZHA, C. S., DUFFY, T. S., HEMLEY, R. J. & MAO, H. K. 2001. Quasi-hydrostatic compression of magnesium oxide to 52 GPa: Implications for the pressure-volume-temperature equation of state. *Journal of Geophysical Research-Solid Earth,* 106**,** 515-528.

SUN, W., YOSHINO, T., KURODA, M., SAKAMOTO, N. & YURIMOTO, H. 2019. H-D Interdiffusion in Single-Crystal Olivine: Implications for Electrical Conductivity in the Upper Mantle. *Journal of Geophysical Research-Solid Earth,* 124**,** 5696-5707.

TOLLAN, P. M. E., SMITH, R., O'NEILL, H. S. C. & HERMANN, J. 2017. The responses of the four main substitution mechanisms of H in olivine to H2O activity at 1050 degrees C and 3 GPa. *Progress in Earth and Planetary Science,* 4.

WANG, Z. Y., HIRAGA, T. & KOHLSTEDT, D. L. 2004. Effect of H+ on Fe-Mg interdiffusion in olivine, (Fe,Mg)(2)SiO4. *Applied Physics Letters,* 85**,** 209-211.

YOSHINO, T., MATSUZAKI, T., SHATSKIY, A. & KATSURA, T. 2009. The effect of water on the electrical conductivity of olivine aggregates and its implications for the electrical structure of the upper mantle. *Earth and Planetary Science Letters,* 288**,** 291-300.

YOSHINO, T., ZHANG, B. H., RHYMER, B., ZHAO, C. C. & FEI, H. Z. 2017. Pressure dependence of electrical conductivity in forsterite. *Journal of Geophysical Research-Solid Earth,* 122**,** 158-171.

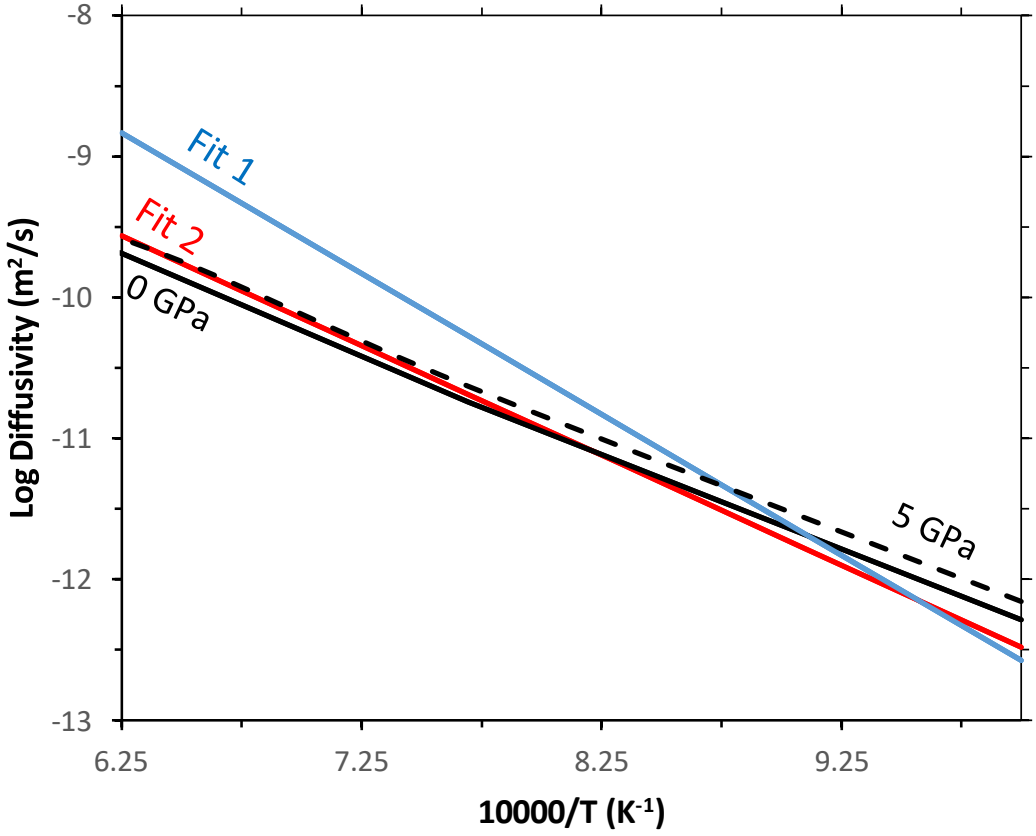

677

678 Figure 1: Comparison of D_{Mg}^{HVac} (diffusivity of $(2H)_{Mg}^{X}$) calculated in this study at 2

679 corrected pressures compared to a value determined from fitting a model to

680 experimental data for H diffusion (Fit 1 and 2, Equation 27 and 28 in Jollands *et al.*

681 (2021).

682

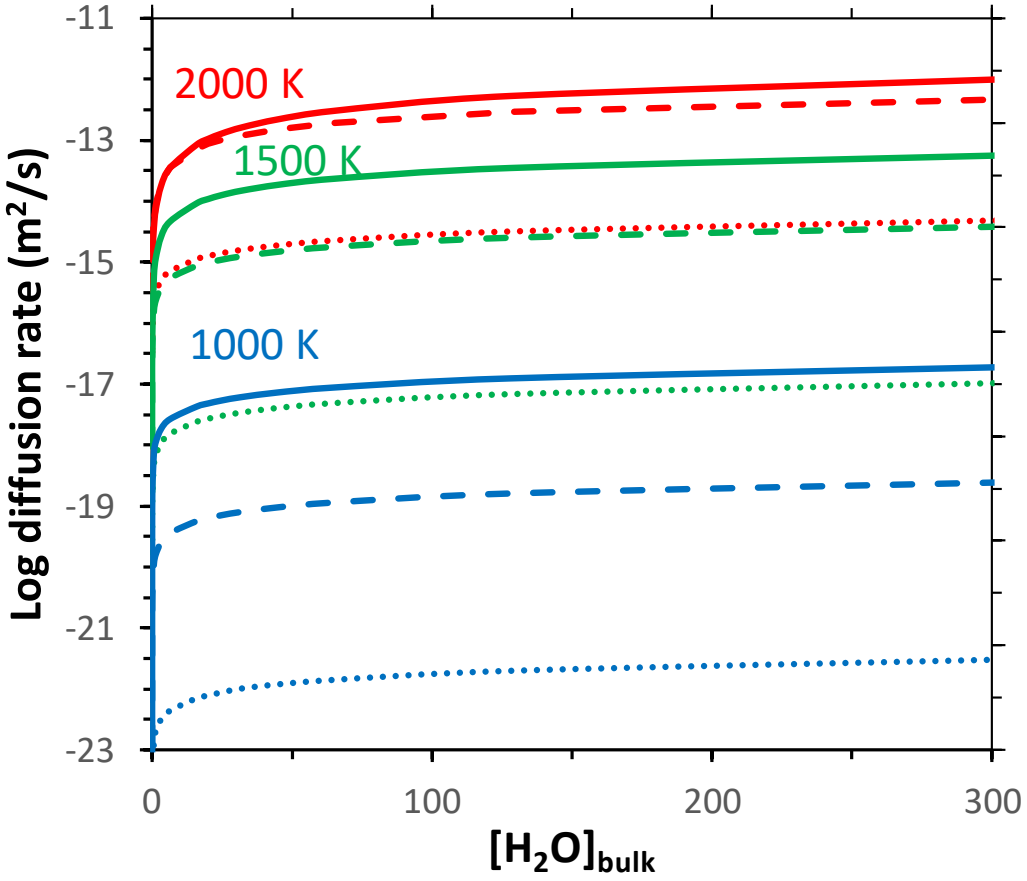

683

684 Figure 2: Predicted diffusion rates in pure forsterite as a function of $[H_2O]_{bulk}$ at three
685 different temperatures (2000 K=red, 1500 K=green, 1000 K=blue) and with three
686 different corrected pressures (0 GPa=solid lines, 5 GPa= dashed line, 10 GPa= dotted
687 lines).

688

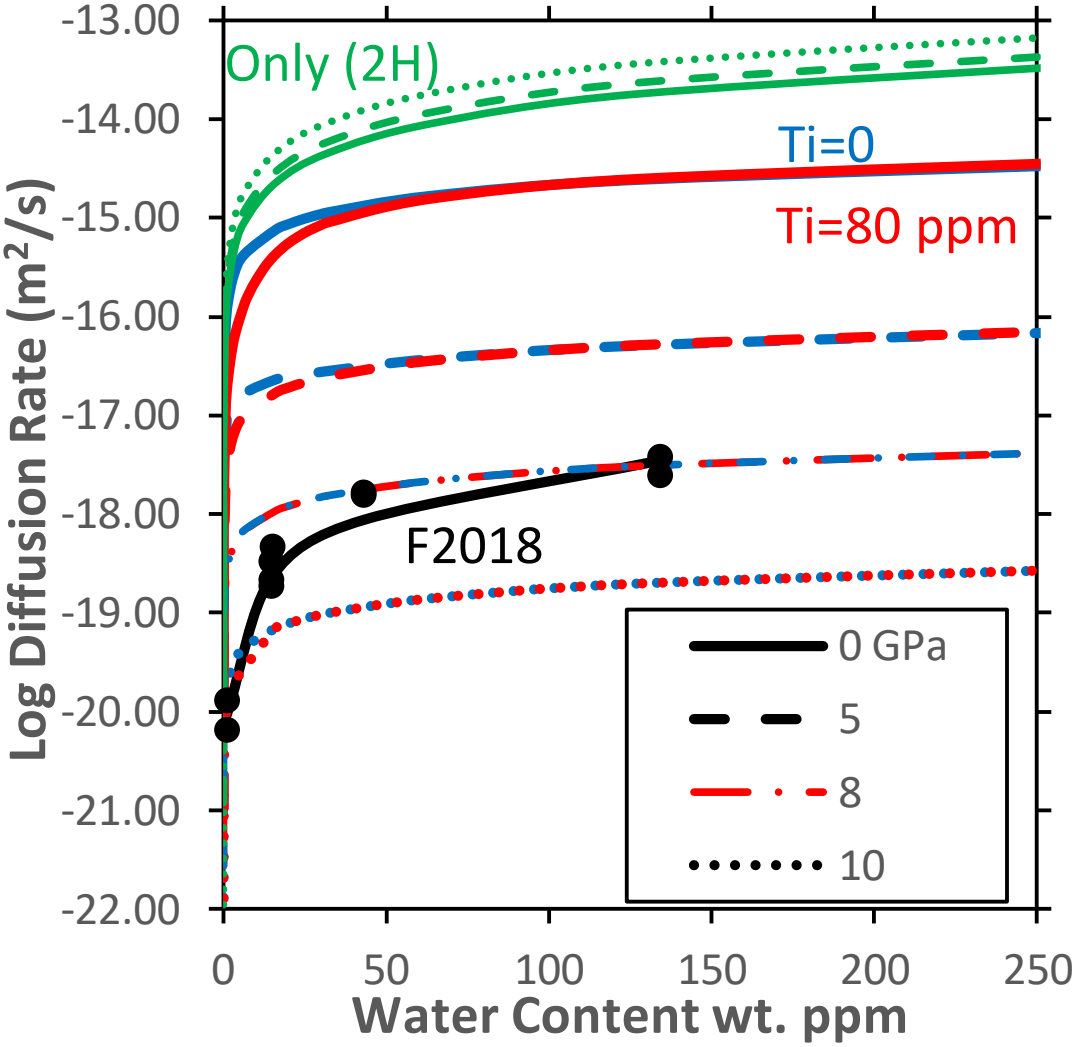

Figure 3: Plot of diffusion rate as a function of water content at 1300 K and at different corrected pressures. Three different sets of data are presented, green where all water is artificially $(2H)^{X}_{Mg}$, blue where the system is solved with no Ti ($(2H)^{X}_{Mg}$ and $(4H)^{X}_{Si}$)) and red where the system is solved with TiO_2= 80 wt. ppm ($(2H)^{X}_{Mg}$, $(4H)^{X}_{Si}$ and $\{Ti^{\cdot\cdot}_{Mg}(2H)''_{Si}\}$). The concentration of Ti was chosen to match that of Fei *et al.* 2018 whose results are presented in black and which were measured at ~1300 K and 8 GPa. The Ti=0 ppm and Ti=80 ppm traces are similar at high water concentrations but diverge at lower water concentrations.

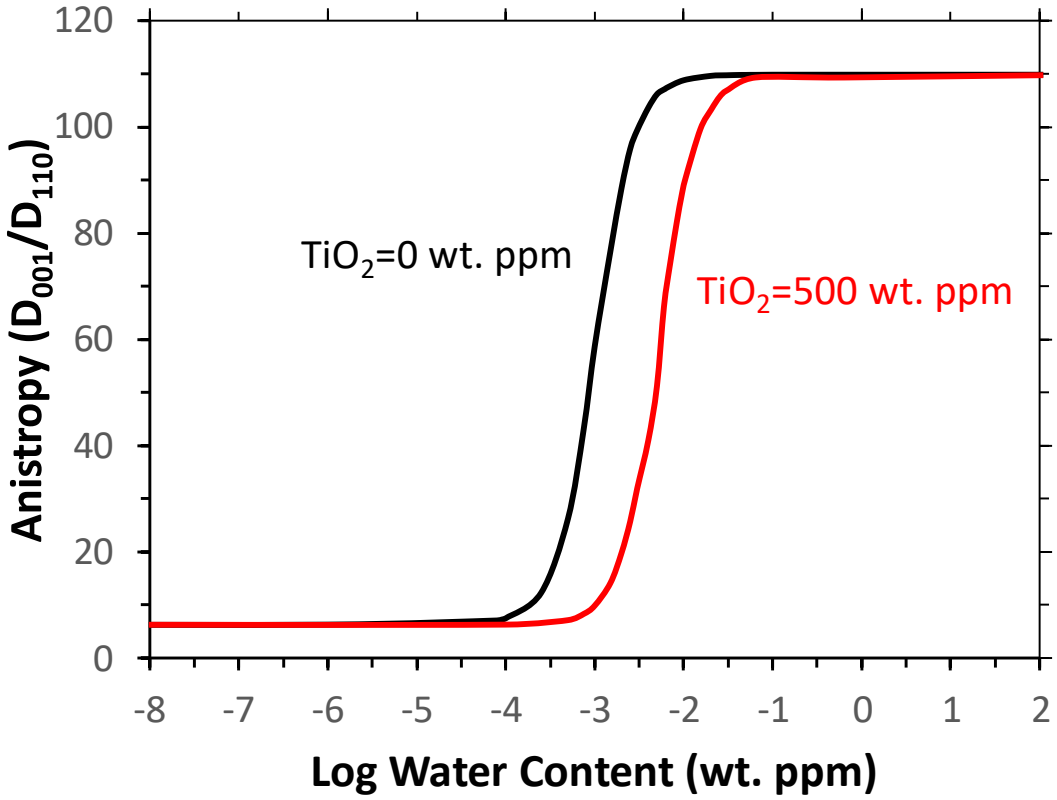

Figure 4 The anisotropy of diffusion [$D_{[001]}/D_{[110]}$] as a function of water content at 1500 K and 0 GPa corrected and with and without TiO_2. At low water contents a "dry" regime persists in which anisotropy is low, at high water contents a "wet" regime in which anisotropy is high. In both regimes the anisotropy is insensitive to water content, only varying in a small transition window between them. All pressure and temperatures gave similar plots with some numbers listed in Table 3.

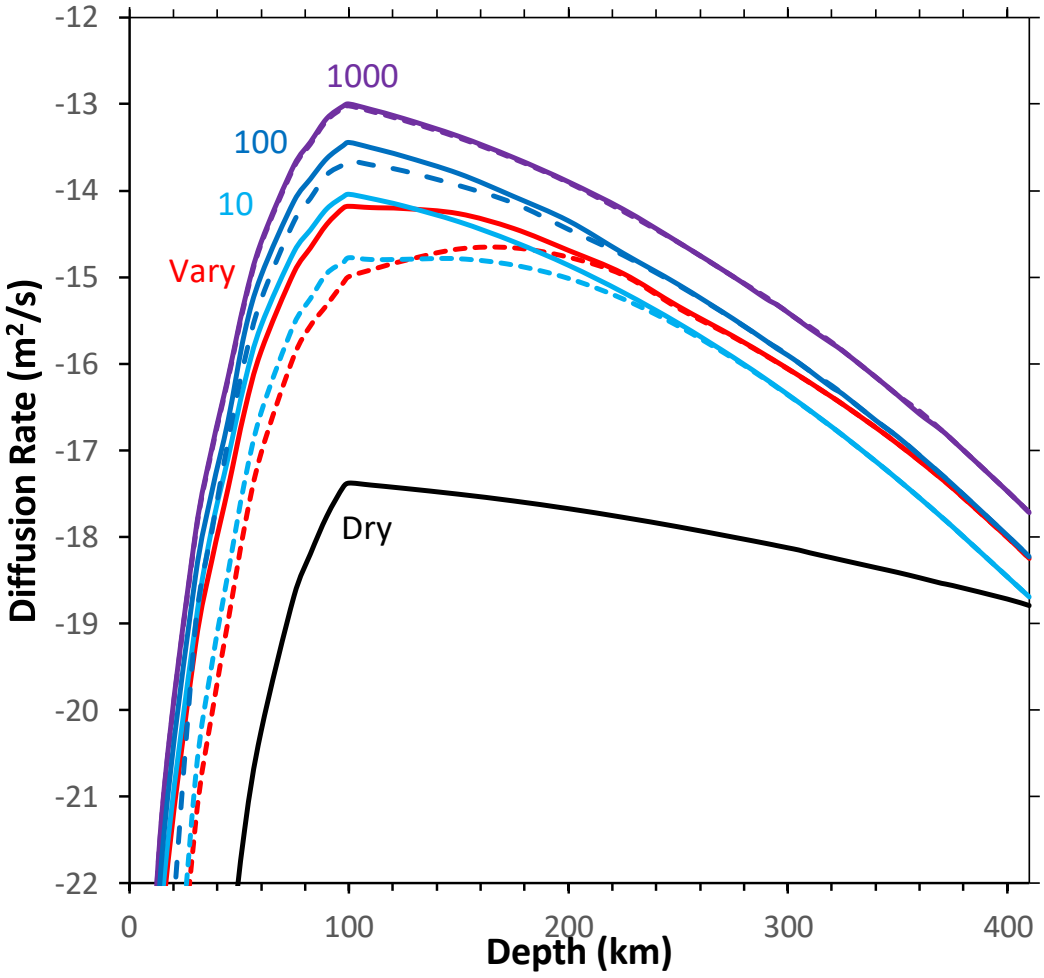

Figure 5 Diffusion rate of Mg along an oceanic geoetherm with different amounts of Ti and water. Solid and dashed lines represent "pure" forsterite and forsterite with 500 wt. ppm TiO_2 respectively along an oceanic geotherm taken from Green and Ringwood (1970) (points in Table S2). The black line contains no H-bearing defects, while shades of blue contain fixed amounts of H-bearing defects (given as $[H_2O]_{bulk}$ in wt. ppm) and red lines have a varying amount of water content with depth $[H_2O_{bulk}] = (3 + 1.6 \times 10^{-4} z^{2.2}$ taken from Demouchy and Bolfan-Casanova (2016) where z is depth in km. Values below 50 km require extrapolation below 1000 K and thus are potentially unreliable.

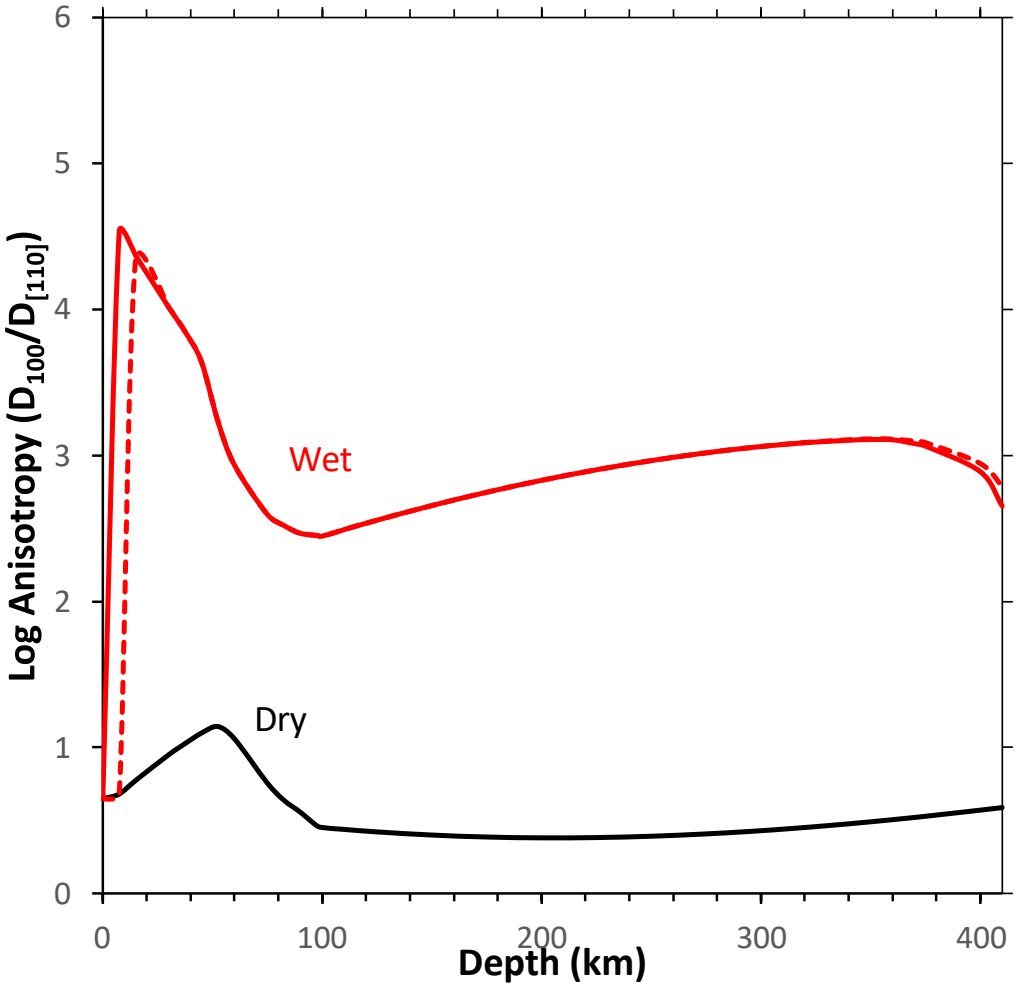

Figure 6 Anisotropy of diffusion [$D_{[001]}/D_{[110]}$] of Mg along an oceanic geotherm**.** Dry forsterite is shown in black wet forsterite is shown in red with the solid line representing no TiO_2 and the dashed line an oceanic geotherm with 500 wt. TiO_2. All amounts of water above 1 wt. ppm produce an identical trace to the varied water curves pictured here (and thus are not shown) as discussed in the text.

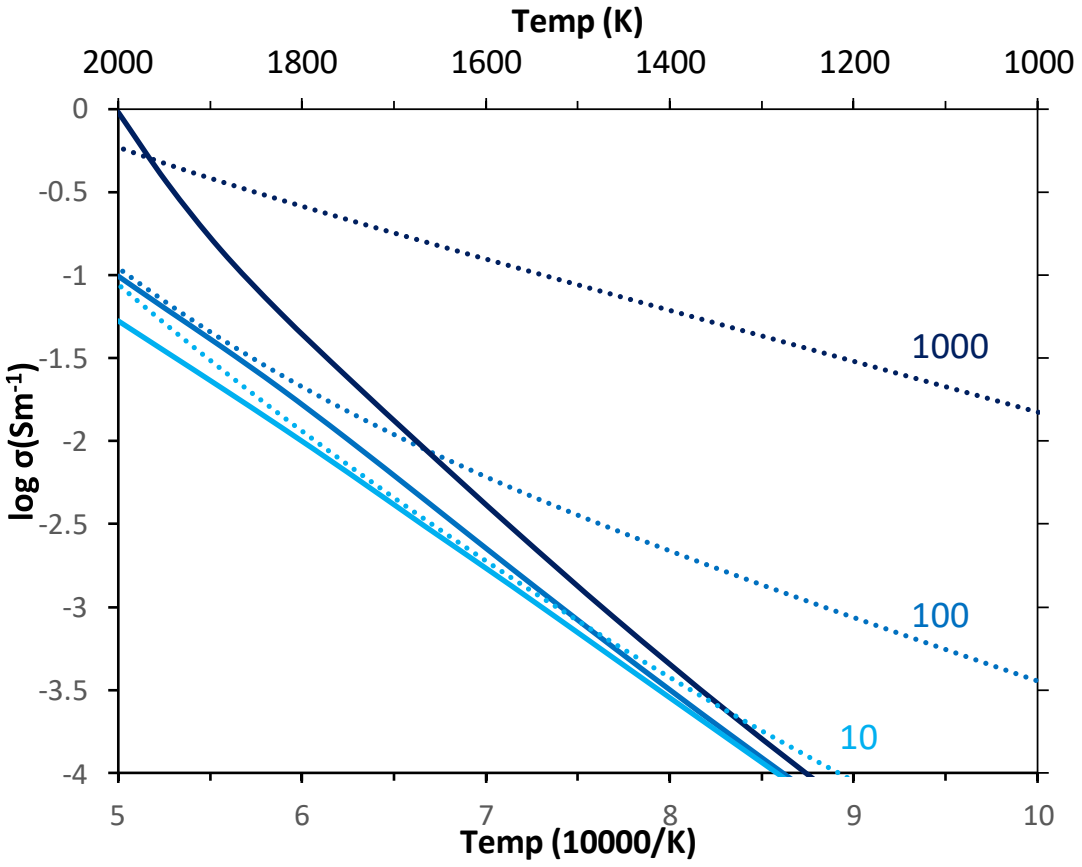

731

732 Figure 7: Plot of conductivity vs temperature for different water concentrations (10,
733 100 and 1000 wt. ppm). Solid lines are our prediction using Equation 6 in the text,
734 the dotted lines are the G14 model which was determined from Equation 1 and Table 1
735 in Gardes *et* al (2014). In Figure S2 we show the results of different modifications to
736 Equation 6 but none of them are close to matching the model of G14**.** Pressure was
737 set to 0 GPa corrected, the effect of pressure is shown in Figure S3.

738

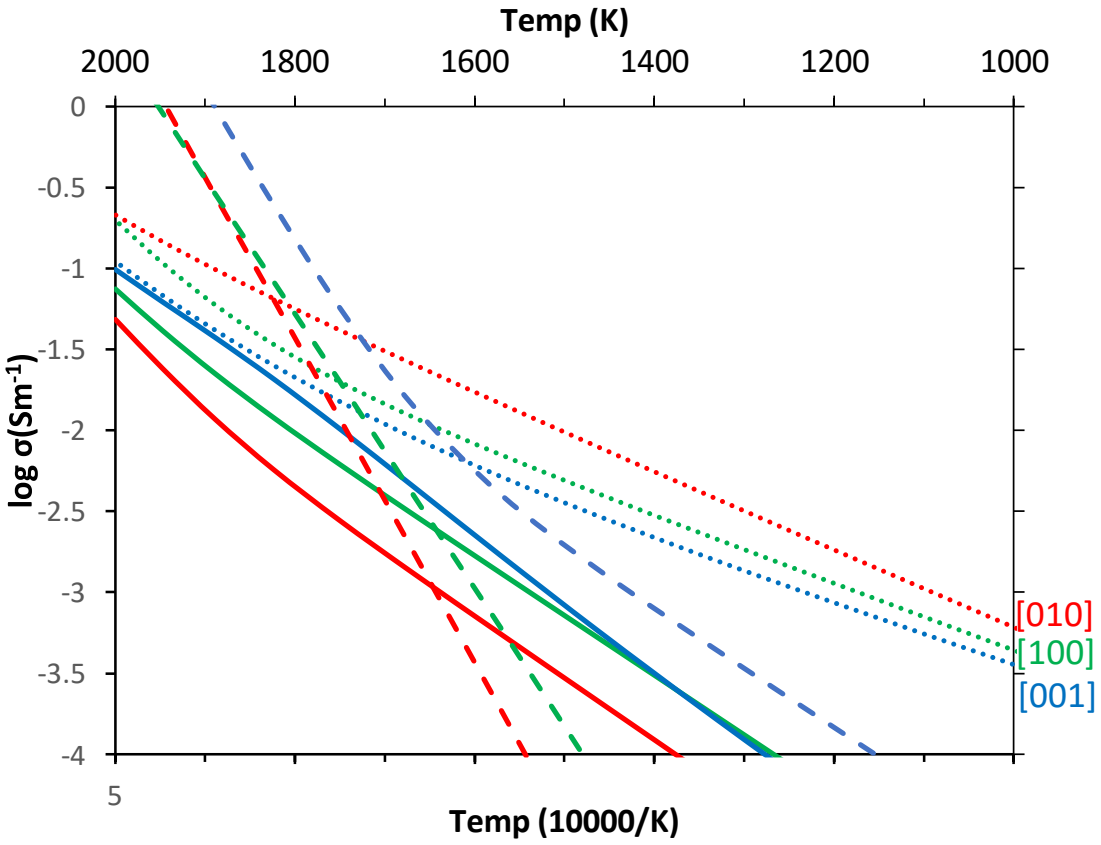

739

740 Figure 8: Comparison of conductivity in three directions (red=[010], green=[100],
741 blue=[001]) against temperature determined from Equation 6 in our model (solid lines)
742 vs those determined from G14 (dotted lines) and from Fei et al. 2020 (dashed lines)
743 determined from Equation 9 and Table 3. $[H_2O]_{bulk}$ was set to 100 wt. ppm and
744 pressure to 0 GPa (corrected). Our predicted diffusional anisotropy is close to the
745 reverse of that determined by Gardes *et al.* 2014 while we match the same order as in
746 Fei et al. 2020.

747

748

		D_{Mg}^{Int}			D_{Mg}^{Vac}			D_{Mg}^{HVac}		
		[100]	[010]	[001]	[100]	[010]	[001]	[100]	[010]	[001]
0 GPa	1000 K	2.94x 10^{-12}	1.16x 10^{-11}	6.13x 10^{-12}	3.92x 10^{-14}	1.64x 10^{-13}	1.88x 10^{-10}	4.70x 10^{-17}	6.49x 10^{-17}	5.17x 10^{-13}
	1500 K	1.23x 10^{-11}	4.45x 10^{-11}	2.07x 10^{-11}	1.89x 10^{-10}	4.99x 10^{-10}	3.63x 10^{-9}	1.34x 10^{-13}	1.12x 10^{-12}	1.24x 10^{-10}
	2000 K	3.09x 10^{-11}	1.06x 10^{-10}	4.37x 10^{-11}	1.24x 10^{-9}	3.24x 10^{-9}	1.52x 10^{-8}	8.70x 10^{-13}	7.49x 10^{-12}	7.19x 10^{-10}
5 GPa	1000 K	2.04x 10^{-11}	9.05x 10^{-11}	6.66x 10^{-11}	7.95x 10^{-14}	2.11x 10^{-13}	1.88x 10^{-10}	4.94x 10^{-18}	6.10x 10^{-18}	6.97x 10^{-13}
	1500 K	5.06x 10^{-11}	1.94x 10^{-10}	9.55x 10^{-11}	2.80x 10^{-10}	6.16x 10^{-10}	3.38x 10^{-9}	2.34x 10^{-14}	2.02x 10^{-13}	1.57x 10^{-10}
	2000 K	9.74x 10^{-11}	3.26x 10^{-10}	1.20x 10^{-10}	1.81x 10^{-9}	3.96x 10^{-9}	1.42x 10^{-8}	1.54x 10^{-13}	1.36x 10^{-12}	9.08x 10^{-10}
10 GPa	1000 K	1.16x 10^{-10}	3.60x 10^{-10}	3.40x 10^{-10}	1.27x 10^{-13}	1.65x 10^{-13}	1.87x 10^{-10}	3.03x 10^{-19}	1.06x 10^{-18}	1.13x 10^{-12}
	1500 K	1.18x 10^{-10}	4.52x 10^{-10}	2.27x 10^{-10}	1.72x 10^{-10}	4.35x 10^{-10}	3.20x 10^{-9}	1.09x 10^{-14}	6.60x 10^{-14}	1.73x 10^{-10}
	2000 K	2.08x 10^{-10}	6.74x 10^{-10}	2.41x 10^{-10}	1.06x 10^{-9}	2.73x 10^{-9}	1.28x 10^{-8}	7.38x 10^{-14}	4.52x 10^{-13}	9.08x 10^{-10}

749 Table 1 Calculated diffusivity coefficients (in m^2s^{-1}) for $Mg_{Int}^{\bullet\bullet}$, Vac_{Mg}'' and $(2H)_{Mg}^{X}$

750 as a function of corrected pressure and temperature.

751

752

753

		1000 K			1500 K			2000 K		
		0 GPa	5 GPa	10 GPa	0 GPa	5 GPa	10 GPa	0 GPa	5 GPa	10 GPa
$[H_2O]_{bulk}$ 1 wt.ppm	$[(4H)_{Si}^{X}]$	-5.46	-5.41	-5.41	-6.46	-5.50	-5.41	-8.02	-6.78	-5.43
	$[(2H)_{Mg}^{X}]$	-6.09	-7.65	-10.82	-5.15	-5.85	-8.46	-5.11	-5.13	-6.52
	$[H_i^{\bullet}]$	-15.94	-15.24	-15.09	-11.51	-14.72	-14.73	-9.00	-12.10	-14.47
	$[V_{Mg}'']$	-15.90	-15.45	-15.32	-11.80	-14.56	-14.57	-8.24	-9.70	-10.35
	$[Mg_i^{\bullet\bullet}]$	-16.16	-16.16	-16.16	-13.93	-14.56	-14.79	-8.28	-9.70	-10.35
$[H_2O]_{bulk}$ 10 wt.ppm	$[(4H)_{Si}^{X}]$	-4.42	-4.41	-4.41	-4.81	-4.44	-4.41	-6.04	-5.00	-4.41
	$[(2H)_{Mg}^{X}]$	-5.58	-7.15	-10.31	-4.32	-5.32	-7.96	-4.12	-4.24	-6.02
	$[H_i^{\bullet}]$	-14.90	-14.99	-15.04	-11.52	-14.68	-14.68	-9.00	-12.10	-14.38
	$[V_{Mg}'']$	-15.16	-15.23	-15.45	-11.81	-14.73	-14.63	-8.98	-10.58	-10.85
	$[Mg_i^{\bullet\bullet}]$	-16.16	-16.16	-16.16	-14.41	-14.74	-14.73	-9.27	-10.58	-10.85
$[H_2O]_{bulk}$ 100 wt.ppm	$[(4H)_{Si}^{X}]$	-3.41	-4.41	-3.41	-3.54	-3.42	-3.41	-4.18	-3.61	-3.41
	$[(2H)_{Mg}^{X}]$	-5.07	-10.32	-9.80	-3.69	-4.81	-7.46	-3.19	-3.54	-5.52
	$[H_i^{\bullet}]$	-13.96	-14.89	-14.98	-11.53	-14.63	-14.63	-9.01	-12.10	-14.30
	$[V_{Mg}'']$	-14.25	-15.15	-15.23	-11.83	-14.81	-14.66	-9.26	-11.26	-11.37
	$[Mg_i^{\bullet\bullet}]$	-16.30	-16.16	-16.16	-14.51	-14.84	-14.69	-10.20	-11.27	-11.37

Table 2: Log of the concentration (in defects/f.u.) of major defects in a system of "pure forsterite" predicted at different temperatures, corrected pressures and water concentrations.

		Dry to Wet		Dry ($[H_2O]_{bulk}$=0 wt. ppm)		Wet ($[H_2O]_{bulk}$=1-300 wt. ppm)			
		Crossover (pure)	Crossover (TiO_2=500 wt. ppm)	log A	log Anisotropy	log A	log B	r	log Anisotropy
1000 K	0 GPa	0.00	0.00	-24.41	1.20	-18.15	-18.10	0.56	3.81
	5 GPa	0.00	0.00	-25.29	0.44	-19.97	-19.99	0.55	4.95
	10 GPa	0.00	0.00	-25.33	0.14	-22.86	-22.91	0.55	5.96
1500 K	0 GPa	0.00	0.01	-17.90	0.80	-15.33	-14.84	0.65	2.04
	5 GPa	0.00	0.00	-18.78	0.60	-15.82	-15.80	0.56	2.89
	10 GPa	0.00	0.00	-19.96	0.57	-18.34	-18.36	0.56	3.40
2000 K	0 GPa	0.58	0.81	-14.51	0.63	-14.34	-14.13	0.88	1.98
	5 GPa	0.35	0.56	-15.26	0.48	-14.45	-14.48	0.67	2.82
	10 GPa	0.85	1.41	-16.32	0.56	-15.68	-15.69	0.56	3.28

Table 3: Various outputs from our diffusion model as a function of corrected pressure and temperature. The first two columns show the concentration (in wt. ppm) of $[H_2O]$ bulk where we convert from the "dry" regime to a "wet" regime defined as the point of inflection in an anisotropy curve such as in Figure 4**.** This is shown for a "pure" forsterite and one containing 500 wt. ppm TiO_2, the value is similar and small in both cases. The final 6 columns concern diffusion rates in "pure" (Ti-free) forsterite with Ti-bearing forsterite shown in Table 4. The first two columns concern dry forsterite with no H-bearing defects and show the diffusion rate (A in Equation 4) and the anisotropy $[D_{[001]}/D_{[110]}]$**.** The last 4 columns concern forsterite with H-bearing defects. We show the results of fitting to Equation 4 between $[H_2O]_{bulk}$ 1 to 300 wt. ppm (the "wet" region)- for the purposes of fitting we used $[H_2O]_{bulk}$ =$[H_2O]_{bulk}$-1 so that A in these cases reflects diffusion at 1 wt. ppm $[H_2O]_{bulk}$. The final column shows the anisotropy of the wet system.

		0 GPa				5 GPa				10 GPa			
	TiO_2 (wt. ppm)	log A (dry)	log A	log B	r	log A (dry)	log A	log B	r	log A (dry)	log A	log B	r
1000 K	0	-24.22	-18.15	-18.10	0.56	-25.29	-19.97	-19.99	0.55	-25.33	-22.86	-22.91	0.56
	100	-24.22	-19.72	-19.15	1.09	-25.29	-20.36	-20.00	0.58	-25.33	-22.93	-22.89	0.56
	500	-24.22	-20.26	-21.11	1.63	-25.29	-21.60	-21.29	1.02	-25.33	-24.68	-23.59	0.91
1500 K	0	-17.90	-15.33	-14.84	0.65	-18.78	-15.82	-15.80	0.56	-19.96	-18.34	-18.36	0.56
	100	-17.90	-15.83	-15.42	0.95	-18.78	-16.08	-15.88	0.59	-19.96	-18.36	-18.32	0.55
	500	-17.90	-16.34	-15.99	1.08	-18.78	-16.83	-16.47	0.96	-19.96	-18.41	-18.32	0.55
2000 K	0	-14.51	-14.34	-14.13	0.88	-15.26	-14.45	-14.48	0.67	-16.32	-15.68	-15.69	0.56
	100	-14.51	-14.39	-14.29	0.95	-15.26	-14.57	-14.55	0.77	-16.32	-15.73	-15.69	0.56
	500	-14.51	-14.61	-14.68	1.05	-15.26	-14.75	-14.66	0.93	-16.32	-15.77	-15.69	0.55

774 Table 4: Plot of fits to dry and wet forsterite (as in Table 3) with varying amounts of
775 TiO_2 added at different T and P. Anisotropy is not affected by the addition of Ti and
776 is presented in Table 3.

777

	Gardes (2014)		This work				
	Fit 1 (r=1/3)	Fit 2 (r=1.99)	1 wt. ppm	10	100	1000	10 (all $(2H)_{Mg}^{X}$)
	ΔH^{Hyd}	ΔH^{Hyd}	ΔH^{Hyd}	ΔH^{Hyd}	ΔH^{Hyd}	ΔH^{Hyd}	ΔH^{Hyd}
[100]	92	66	299.64	283.77	273.55	260.86	348.75
[010]	95	104	367.38	346.67	324.35	278.70	336.99
[001]	81	61	377.20	353.38	327.66	279.30	268.45

Table 5: Comparison of the activation energy (in kJ/mol) in three directions for the hydrous part of the conductivity fit in Gardes *et al.* 2014 with that determined in this work at 0 GPa (corrected). Two fits from Gardes *et al*. 2014 are shown with different water exponents (r). To determine our activation energy we determined conductivity between 800-2000 K while setting the polaron term in Equation 6 to 0 and then fit an equation of the form $\sigma = ae^{-b/RT}$ where a and b are fitting parameters. This was done at multiple different values of $[H_2O]_{bulk}$. The final column represents $[H_2O]_{bulk}$ =10 wt. ppm but with all water fixed as $(2H)_{Mg}^{X}$.